Investigation of microstructure and hardness of a rib geometry produced by metal forming and wire-arc additive manufacturing

Markus Hirtler[1,*], *Angelika* Jedynak[1], *Benjamin* Sydow[1], *Alexander* Sviridov[1], and *Markus* Bambach[1]

[1]Brandenburg University of Technology Cottbus-Senftenberg, Chair of Mechanical Design and Manufacturing, 03046 Cottbus, Germany

Abstract Within the scope of consumer-oriented production, individuality and cost-effectiveness are two essential aspects, which can barely be met by traditional manufacturing technologies. Conventional metal forming techniques are suitable for large batch sizes. If variants or individualized components have to be formed, the unit costs rise due to the inevitable tooling costs. For such applications, additive manufacturing (AM) processes, which do not require tooling, are more suitable. Due to the low production rates and limited build space of AM machines, the manufacturing costs are highly dependent on part size and batch size. Hence, a combination of both manufacturing technologies i.e. conventional metal forming and additive manufacturing seems expedient for a number of applications. The current study develops a process chain combining forming and additive manufacturing. First, a semi-finished product is formed with forming tools of reduced complexity and then finished by additive manufacturing. This research investigates the addition of features using AlSi12 created by Wire Arc Additive Manufacturing (WAAM) on formed EN-AW 6082 preforms. By forming, the strength of the material was increased, while this effect was partly reduced by the heat input of the WAAM process.

Keywords: Additive Manufacturing, Metal forming, Microstructure

1 Introduction

The demand for individualized products is a significant driver for improvements of manufacturing processes. The costs for conventional fabrication, e.g. by closed-die forging, rises with increasing complexity and decreasing batch-size [1]. A short cycle time is beneficial for die-based forming processes, making them economical for large-scale production. For the production of customized parts or small batches, the tooling costs are unacceptably high. Additive manufacturing (AM) methods do not rely on dedicated tools, and hence, allow for the production of single parts or small batch sizes irrespective of the complexity. Currently available powder-based AM processes show a low deposition rate of 0.3 kg/h [2] for Selective Laser Melting (SLM) and 3.0 kg/h [3] for Laser Metal Deposition (LMD). A more promising technology is Wire Arc Additive Manufacturing (WAAM) with higher deposition rates of up to 10 kg/h [4], good power efficiency and low investment costs [5].

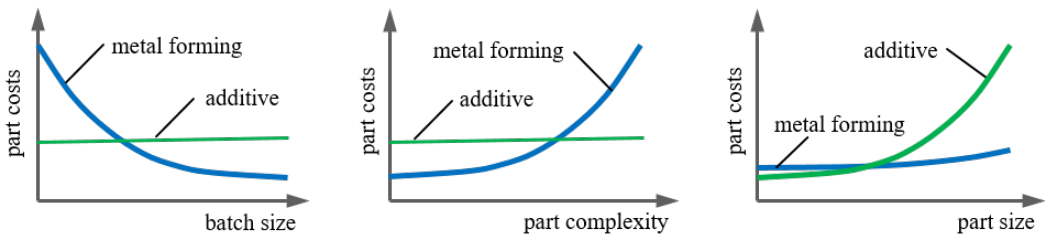

Fig. 1. Comparison of part costs for metal forming and additive processes regarding batch size, part complexity and part size.

* Corresponding author: markus.hirtler@b-tu.de

However, resolution and surface roughness of SLM are better than WAAM [6]. With both methods, nearly full density can be achieved [7]. The dependence of part costs on part size, part complexity and batch size are illustrated schematically in Fig. 1. Instead of using a single technology for manufacturing the desired part shape, a combination of processes could be beneficial for manufacturing smaller batch sizes or product variants. One reasonable synergy can be obtained by combining wire arc additive manufacturing and metal forming, yielding two possible process routes, which are visualized in Fig. 2. First, an additive manufacturing process, e.g., WAAM can be used to generate a pre-shaped semi-finished part. The semi-finished part will then be formed by using a single forming tool to achieve the final contour.

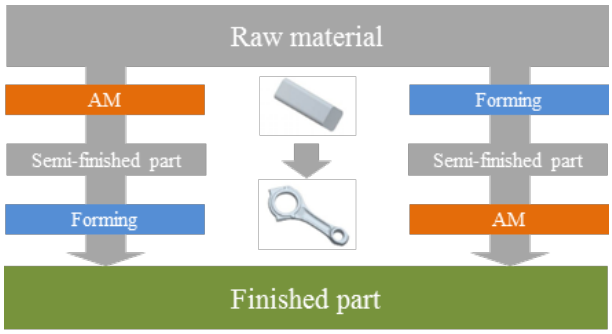

Fig. 2. The two possible routes and combinations of AM and metal forming processes.

Behrens et al. investigated deposited claddings on a shaft which was formed subsequently [8]. The hybrid part was made of a 42CrMo4 bar cladded with the high-alloyed steels 1.8401 and 1.4718. The forming processes applied were forging and cross-wedge-rolling (CWR). It was found that the cladded part remains undamaged after forging and CWR causes a significant reduction of pores.
Another process route was examined by Zhang et al. where SLM was used to fabricate Ti6Al4V preforms for forming [9]. The microstructure was improved and anisotropy was minimized after forming and subsequent heat treatment. A reduction of porosity was obtained by high deformation rates and a high degree of deformation, which also leads to higher fatigue strength. Previous work of Bambach and Sizova [10] focused on the forming of AM-pre-forms made of Ti6Al4V and Inconel 718 [11]. A good formability of both materials was observed in the 3D printed state, with lower activation energy for hot forming. Williams et al. used WAAM to produce a wing spar from aluminum, which was generated on sheet metal, but without strength-enhancing forming [4]. Martina et al. used WAAM to produce Ti6Al4V parts and realized local forming by rolling during the AM process [12]. They found that the local forming leads to grain refinement of the primary β-grains, a thickness reduction of the α-phase lamellae and a change from a columnar to an equiaxed microstructure.

The second process route utilizes a conventionally pre-formed part, which misses features of the final workpiece. These features, such as cooling or reinforcement ribs or other structural or functional elements are then added via AM.
Bambach et al. [13] showed that AM can be used to create local reinforcements on sheet metal parts. Extensive work on additively manufactured features which are added to formed parts have been performed by Merklein et al. [14–17]. While most existing work focusses on additive manufacturing of features on pre-formed sheet metal parts, this work examines the WAAM of stiffening ribs created by forging. Forging of features such as ribs with large aspect ratios is problematic, especially on hydraulic presses with their long contact times between tool and workpiece. A possibility to overcome limitations of the forging process is to decrease the complexity of the forged shape and to add the respective feature by WAAM.

2 Methodology

The geometry used for the current study is presented in Fig. 3 and represents a forged T-section with a length of 120 mm. The width of the rib is 20 mm. In the forging process, a rib height of 50 mm can be achieved. Higher ribs cause a much higher tool wear and increase the probability of forging defects. Using WAAM, the height of the bridge was expanded to a total of 95 mm. As reference, T6-heat treated EN-AW 6082 bulk material was used which was milled to a T-section geometry with a cross section of 120 mm x 50 mm x 20 mm. On the rib of this section, AlSi12 was added using WAAM.

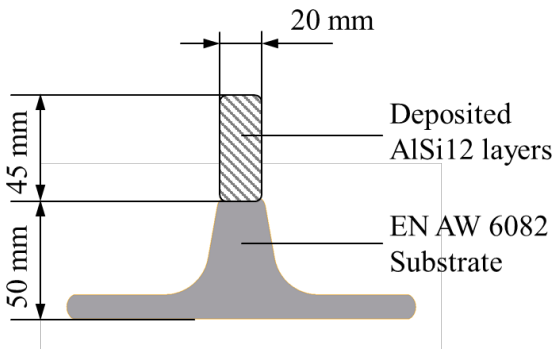

Fig. 3. Geometry of the forged sample with added AM structure.

The aluminum alloy EN-AW 6082 was used as substrate material and AlSi12 was used as a filler metal for the demonstration of the combined forming and AM process. The chemical composition of both materials is presented in Table 1 and Table 2, respectively.

Table 1. Chemical composition of EN-AW 6082 in wt%. [18]

Si	Mg	Mn	Fe	Cr	Zn	Cu	Ti
0.80	0.66	0.41	0.43	0.02	0.06	0.05	0.01

Fig. 4. Processing stages of samples. Left: forged, middle: machined, right: deposited AM layers.

Table 2. Chemical composition of AlSi12 in wt%. [19]

Si	Fe	Cu	Zn	Mn	Mg	Ti
12.0	<0.6	<0.3	<0.2	<0.15	<0.1	<0.15

The temperature of the samples was continuously monitored during the forming and the additive manufacturing process with thermocouples. The position of the thermocouple during the AM process is marked in Fig. 6. The maximum recorded temperature during the deposition of the AM layers was 460 °C and this value occurs during the deposition of the first layers. For the deposition of the subsequent layers, an average temperature between 270 °C and 325 °C was recorded.
From the sample geometry, test specimens were extracted for hardness, porosity and microstructure measurements at three distinct positions (substrate material, joining zone and additive layer).

2.1 Production of samples

The three stages (forged, machined, deposited AM layers) of a specimen are illustrated in Fig. 4. After the forging process and the heat treatment the top side was milled to obtain a flat top, which improves the welding process.

2.1.1 Forming and heat treatment

The setup for the forming process can be seen in Fig. 5. A round bar of EN-AW 6082 with a diameter of 75 mm was used as billet. After the forming process the true plastic strain in the middle of the part was between 0.5 and 1 and ~2.6 at the edge of the part.

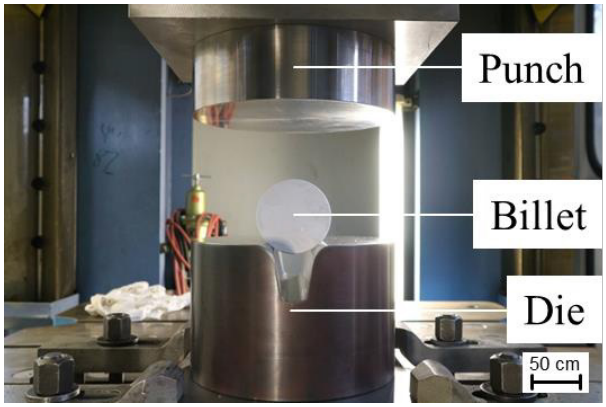

Fig. 5. Setup for the forming process.

The forming parameters are listed in Table 3.

Table 3. Forming parameters.

Punch speed	40 mm/s
Starting temperature	500 °C
Max. Force	3167 kN
Lubrication	Boron nitride

After forming a subsequent heat treatment including solution annealing at 530±10 °C for 2 hours, quenching in water and a subsequent aging at 165±5 °C for 10 hours was performed.

2.1.2 Wire+arc additive manufacturing

A six-axis FANUC® robot with the welding power source TPS/i 500 by Fronius® was used to deposit the layers on the substrate material. The wire had a diameter of 1.2 mm. The shielding gas was pure Argon with a gas flow rate of 15 l/min. The applied WAAM process parameters are presented in Table 4. The seams were deposited in longitudinal direction next to each other. Because of the thicker material base, the forged parts were preheated up to 190 °C while the thinner reference material was held at 65° C from the beginning of the welding process.

Table 4. Process parameters for WAAM.

Layer	1st	2nd	3rd	≥ 4th
Wire feed rate [m/min]	7.1	6.3	6.1	6.0
Current [A]	140	105	96	91
Voltage [V]	15.0	14.0	13.7	13.6

2.2 Investigations

The hardness, microstructure and porosity were analyzed to access the impact of the process combination on the mechanical properties. Fig. 6 shows the locations of the extracted specimens, separated into three zones: (1) AM zone, (2) interface zone and (3) substrate zone. For each zone, one or more micro sections were cut from the specimens. These micro sections were extracted not only from the middle but also from the edge. For microscopic analysis, the samples were etched with a Keller reagent and examined by means of a light optical microscope. Porosity was determined with the software ATLAS by TESCAN. The hardness was measured via two methods

i.e. the Vickers hardness test and the Ultrasonic Contact Impedance (UCI) with a BAQ UT100-V device both under conditions of HV 0.5.

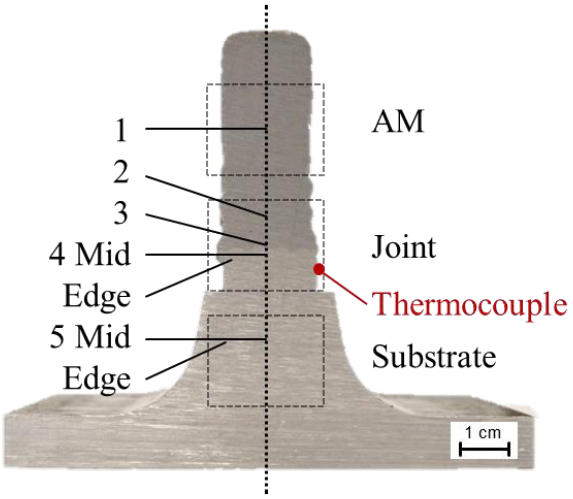

Fig. 6. Positions of specimen extraction for metallography. Pos. 1: AM layers; Pos. 2-4: interface zone with Pos. 3 as interlace area and Pos. 5: substrate. Position of thermocouple for temperature measurement

3 Results

3.1 Microstructure/Porosity

The AM layers show the development of columnar dendritic grains (see Fig. 7). The orientation of the grains is similar for formed & welded (FW) and milled & welded parts (MW) at Pos. 1. Formation of highly oriented columnar dendrites is an indication of a low temperature gradient. A similar structure for welded EN AW 6082 was also identified by Babu et al. [20]. The increasing part height leads to reduced heat conduction and the repetitive heating of previously deposited layers to additional continuous thermal energy input.

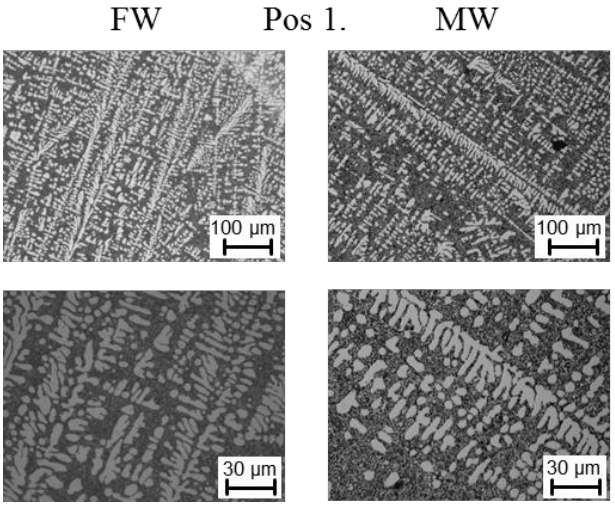

Fig. 7. Microstructure of the additive manufactured layers at Pos. 1. FW – formed and welded, MW – milled and welded.

Fig. 8 shows Pos. 2 slightly above the bonding zone. Compared to Pos. 1 it can be seen that the dendritic structure is less oriented. The crystal growth reduces the amount of elongated grains caused by the repeated heating during the welding process.

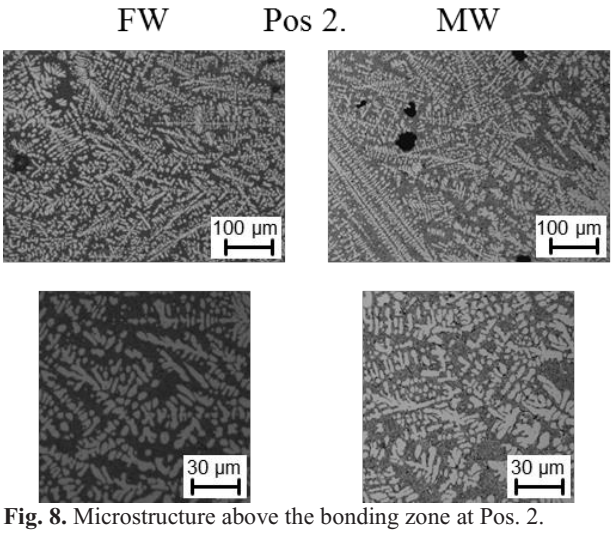

Fig. 8. Microstructure above the bonding zone at Pos. 2.

The mid bonding zone (Pos. 3) is illustrated in Fig. 9. The direction of grain growth of the primary phase is oriented along the largest temperature gradient, which induces the formation of a narrow columnar zone with mainly α-Al grains and eutectic Al-Si-structures lying in-between at the boundary layer. The top area of the T-section was not governed by the forming process as indicated by the coarse grain structure. As mentioned the FW part was preheated for the AM process. The thinner MW part caused a high cooling rate during the deposition of the first AM layers. This results in a globular grain formation.

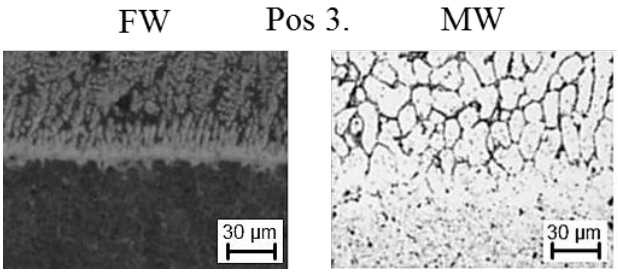

Fig. 9. Microstructure of interface area at Pos. 3. Top: AM layer, bottom: substrate.

In Fig. 10 the microstructure of the edge and mid area for a FW part is displayed. The elongation caused by forming can be seen in the edge area of the part while the mid position is less deformed. The microstructure of the MW part consists of fine grains, which is also reported by Kumar et al. [21].

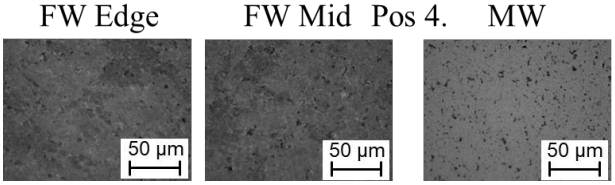

Fig. 10. Microstructure of bottom bonding zone

The microstructure of the substrate is illustrated in Fig. 11. The substrate was less affected by the heat input. This shows that the formed structured remains in the same condition if the location of the heat input is not in close vicinity. Thus, mechanical properties such as tensile strength should remain unaffected.

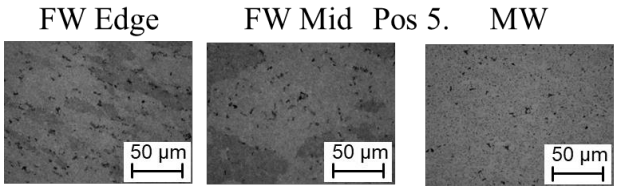

Fig. 11. Microstructure of substrate.

The results for the porosity are presented in Table **5**. It can be seen that the obtained porosity shows no difference between FW and MW in the pure AM or substrate zone. For the interface area the porosity reaches about 1.0 %. In general, the welding of aluminum is difficult due to take-up of hydrogen, as molten aluminum has a much higher solubility than solidified aluminum. The maximum value of 1.2 was measured directly in the interface zone. The porosity during deposition of subsequent layers is below 1.0 %. This value is the limit for additive manufacturing processes according to VDI3405 [22]. There were no hot cracks detected in the samples.

Table 5. Porosity for FW and MW in %.

Area	Pos.	FW	MW
AM	1	0.6	0.6
	2	1.2	1.2
Joint	3	1.0	<0.1
	4	<0.1	<0.1
Substrate	5	<0.1	<0.1

3.2 Hardness

The obtained hardness values are shown in
Fig. 12. The hardness of the non-forged base material was 40 ± 2 HV. After the transition area, the hardness increased by the fine eutectic structure. In the AM zone, the value stabilized at 55 ± 4 HV, which is in good agreement with the norm values of 52-56 HV (50-55 HB) [23; 24]. The hardness in the AM zone of the forged parts was nearly the same i.e. 61 ± 5 HV. However, the first two AM layers have higher values up to 120 HV which could have been caused by a formation of fine eutectic phase due to a locally higher solidification rate [25]. On the other side, the hardness was only 70 HV in the transition area. At around 10 mm distance to the transition area, the hardness level increased from 70 to 80 HV. A similar effect was also reported by Benoit et al. [26] in their arc welding experiments. This is probably triggered near to the heat-affected zone in the first layers. In the lower forged material the hardness has a range of 57-70 HV, which can also be impacted by the heat effect during the deposition of the AM material.

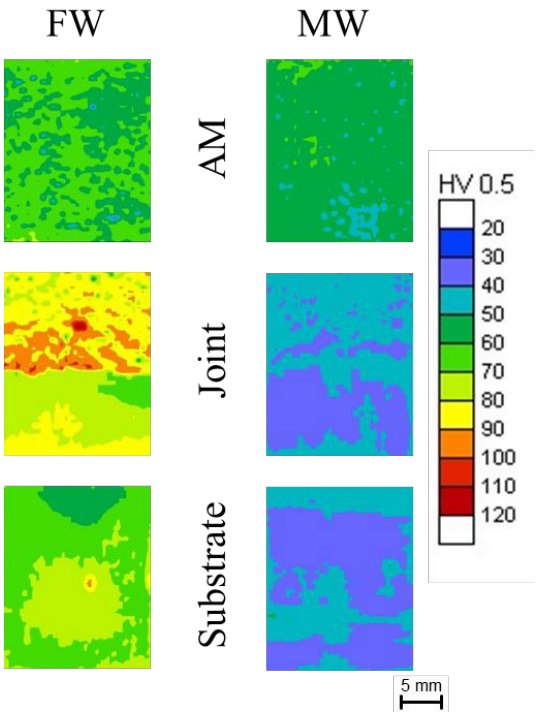

Fig. 12. Hardness distribution for the three areas.

4 Conclusion

It was shown that the additive deposition of layers with a WAAM process on a pre-formed Aluminum component is feasible. The forging process induced a higher hardness in the base material while the hardness of the milled material dropped. Further investigations of the material bonding especially in the 1st AM material layer are needed to enhance the process chain. This demands an improvement of the AM process, as a reduction of the hardness since large hardness gradients may diminish the part strength. The porosity with a maximum of 1.2 % also degrades the mechanical properties, but is in the standard range of welding processes. In further studies, an accurate temperature control and optimized process parameters have to be established. While dissimilar aluminum alloys were used in this study, attempts with EN-AW6082 wire for WAAM will be made to avoid differences in material properties. Other additive manufacturing methods such as laser metal deposition will also be examined for the suitability for a process combination.

The authors thank the European Regional Development Fund (ger. Europäischer Fond für Regionale Entwicklung, EFRE) under the project number 85002924 for the support.

5 References

1 D. Bauer, K. Borchers, T. Burkert, et al., *Handlungsfelder Additive Fertigungsverfahren* (Verein Deutscher Ingenieure, Düsseldorf, 2016).

2 S. Bremen, D. Buchbinder, W. Meiners, et al., LTJ, **6**, 24–28 (2011).

3 K. Shah, I. u. Haq, A. Khan, et al., Materials & Design (1980-2015), 531–538 (2014).

4 S. W. Williams, F. Martina, A. C. Addison, et al., Materials Science and Technology, **7**, 641–647 (2015).

5 O. Yilmaz, A. A. Ugla, Proceedings of the Institution of Mechanical Engineers, Part B: Journal of Engineering Manufacture, **10**, 1781–1798 (2016).

6 A. Gebhardt, *Generative Fertigungsverfahren* (Hanser, München, 2016).

7 Alphons Anandaraj Antonysamy, *Microstructure, Texture and Mechanical Property Evolution during Additive Manufacturing of Ti6Al4V Alloy for Aerospace Application* (Manchester).

8 B.-A. Behrens, L. Overmeyer, A. Barroi, et al., Prod. Eng. Res. Devel., **6**, 585–591 (2013).

9 Q. ZHANG, Z.-l. LIANG, M. CAO, et al., Transactions of Nonferrous Metals Society of China, **5**, 1036–1042 (2017).

10 I. Sizova, M. Bambach, Procedia Engineering, 1170–1175 (2017).

11 M. Bambach, I. Sizova, F. Silze, et al., Journal of Alloys and Compounds, 278–287 (2018).

12 F. Martina, P. A. Colegrove, S. W. Williams, et al., Metall and Mat Trans A, **12**, 6103–6118 (2015).

13 M. Bambach, A. Sviridov, A. Weisheit, et al., Metals, **12**, 113 (2017).

14 M. Merklein, P. Dubjella, A. Schaub, et al., *Interaction of Additive Manufacturing and Forming* (Nürnberg).

15 M. Merklein, D. Junker, A. Schaub, et al., Physics Procedia, 549–559 (2016).

16 A. Schaub, B. Ahuja, L. Butzhammer, et al., Physics Procedia, 797–807 (2016).

17 J. Domblesky, F. F. Kraft, Journal of Materials Processing Technology, **1-3**, 82–86 (2007).

18 Estral Forme d`Alluminio estruse a Misura, *Inspection certificate EN AW 6082 - Doc. Nr. 119669* (2017).

19 MIGAL, *Datenblatt - AlSi12*, http://www.migweld.de/produkte/aluminium-schweissdraht/ml-4047-alsi12/.

20 N. K. Babu, M. K. Talari, D. Pan, et al., Materials Chemistry and Physics, **2**, 543–551 (2012).

21 R. Kumar, U. Dilthey, D. K. Dwivedi, et al., Materials & Design, **2**, 306–313 (2009).

22 VDI, *VDI 3405 Additive Fertigungsverfahren - Grundlagen, Begriffe, Verfahrensbeschreibungen* (Beuth, Berlin, 2014).

23 DIN, *Metallische Werkstoffe – Umwertung von Härtewerten (ISO 18265:2013)* (Beuth, Berlin, 2014).

24 Metallgießerei Chemnitz GmbH, *Übersicht über die gebräuchlichen Gußlegierungen und ihre Eigenschaften*, http://www.metallgiesserei.biz/wordpress/wp-content/uploads/2010/11/Legierungstabelle-DIN-EN-1706-Aluminium-2014.pdf.

25 G. P. Dinda, A. K. Dasgupta, S. Bhattacharya, et al., Metall and Mat Trans A, **5**, 2233–2242 (2013).

26 A. Benoit, P. Paillard, T. Baudin, et al., Science and Technology of Welding and Joining, **1**, 75–81 (2014).